Advances in Aircraft and Spacecraft Science, *Vol. 11, No. 2 (2024) 129-152*
https://doi.org/10.12989/aas.2024.11.2.129

Nonlinear bending analysis of bidirectional graded porous plates with elastic foundations relative to neutral surface

Amr E. Assie*[1,2]

[1]*Department of Mechanical Engineering*, *Faculty of Engineering*, *Jazan University*, *Jazan*, *Saudi Arabia*
[2]*Department of Mechanical Design and Production*, *Faculty of Engineering*, *Zagazig University*, *Zagazig*, *Egypt*

(Received December 11, 2023, Revised July 8, 2024, Accepted July 12, 2024)

Abstract. The applicability of a novel incremental-iterative technique with 2D differential/integral quadrature method (DIQM) in analyzing the nonlinear behavior of Bi-directional functionally graded (BDFG) porous plate based on neutral surface is verified in the present works. A formulation of four variables high shear deformation theory is used to describe the kinematic relations with respect to neutral surface rather than mid-plane. Bi-directional material distributions are presented by power functions through both thickness and axial directions. Porosities and voids are distributed by different cosine functions. The large deformations are included within the sense of nonlinear von Kármán strains. The integro-differential equilibrium equations with associated modified boundary conditions are solved numerically and iteratively by using 2D DIQM. Model validations and parametric analysis are depicted to present the influence of neutral axis, nonlinear strains, gradation indices, elastic foundations, and modified boundary conditions on the static deflection in addition to normal and shear stresses. The proposed model is effective in analyzing the static behavior of many real applications in nuclear reactors, marine and aerospace structures with large deformations.

Keywords: 2D differential integral quadrature method; incremental iterative technique; neutral surface; nonlinear coupled partial differential equations; nonlinear static analysis; Porous BDFG plate

1. Introduction

Functionally graded materials (FGMs), reported by a research group in Japan 1983 (Alshorbagy *et al.* 2011), is an advanced composites type. FGMs are fabricated by designing microstructures, material porosity and their volume fractions to achieve a continuous variation in material, hence, allow to better stress spreading, lower stress concentration and superior thermal resistance capabilities, properties (Xu *et al.* 2023). FGMs are broadly examined by inventors and engineers worldwide, since lots of articles on these materials can be found, Nguyen *et al.* (2018). In specific advanced applications used FGMs as constituents need to grade materials through two/three dimensional rather than 1D to conquer the stress concentration and thermal stresses, (Assie *et al.* 2023a, Shanab and Attia 2022).

Considering bi-directional function graded materials, Qian and Ching (2004) designed a thick two constituent BDFG cantilever plate using the meshless local Petrov–Galerkin method and the

*Corresponding author, Professor, E-mail: aalsaid@jazanu.edu.sa, amr_assie@yahoo.com

http://www.techno-press.org/?journal=aas&subpage=7 ISSN: 2287-528X (Print), 2287-5271 (Online)

higher-order shear deformation plate theory. Lezgy-Nazargah (2015) studied the thermomechanical behavior of structures made of BDFGMs using refined high order global–local theory. Huynh *et al.* (2017) used isogeometric analysis to portray the material property and investigate the free vibration of BDFG Timoshenko beam. Haciyev *et al.* (2018) examined the vibration of BDFG orthotropic plates resting on the two-parameter elastic foundation by using Galerkin method. Hong (2020) studied nonlinear bending and vibration analysis of BDFG porous plate using finite element method. Karamanli *et al.* (2021) presents a comprehensive numerical analysis by finite element of the multi-directional FG strain gradient microplates based on a quasi-3D shear and normal deformation plate theory. Farzam and Hassani (2022) investigated the buckling, and free vibration of functionally graded reduced graphene oxide reinforced nanocomposite plates employing isogeometric analysis. Attia *et al.* (2022) predicted the closed-form solution for natural frequencies of BDFG modified couple stress microbeams subjected to thermomechanical loads. Gupta and Chalak (2022) predicted vibration response of functionally graded sandwich plates by zig-zag theory. Patil and Kadoli (2022) presented the effect of porosity and gradation of Galfenol-D on vibration suppression of BDFG beam by using a differential quadrature technique. Kumar *et al.* (2022) developed a meshfree approach for flexure analysis of BDFG plate subjected to different types of transverse loading. Daikh *et al.* (2023) analyzed analytically the static problem of inhomogeneous BDFG nanoplates using microstructure-dependent higher-order shear deformation theory. Karamanli *et al.* (2023) developed a higher order finite element model to explore the transient vibration of BDFG porous microplate under harmonic moving loads. Melaibari *et al.* (2023) presented mathematical formulation of the dynamical behavior BDFG porous plate resting on a Winkler–Pasternak foundation using unified higher-order plate theories. Ramteke and Panda (2023) predicted the nonlinear static and dynamic response BDFG doubly curved panel by using finite element method.

FGM material is noticeably nonhomogeneous for moderate gradient indices and apparently unsymmetrical about the midplane, so neglecting the true position of the neutral plane causes significant error in the mechanical response evaluation (Eltaher *et al.* 2013, 2014). The following articles considered the physical neutral surface in their analyses. Zhang and Zhou (2008) studied the nonlinear bending response of FG thin plates. Yin *et al.* (2013), Zhang (2013) modeled and analyzed FGM rectangular plates to study the free vibration response. Nguyen *et al.* (2015) used a refined higher-order shear deformation theory for bending, vibration and buckling analysis of FG sandwich plates. Van Do *et al.* (2017) adopted the variational phase field model to study the thermal buckling for cracked FG plates. Fernando *et al.* (2018) presented a formulation based on a reference plane to calculate the vibration frequencies of laminated beams where the end immovable supports are placed at different heights. Esen *et al.* (2018) and Esen (2019a, b) studied the dynamic response of a functionally graded Timoshenko beam on two-parameter elastic foundations due to a variable velocity moving mass under thermal environments. Babaei *et al.* (2019) estimated the large amplitude of free vibrations of long FGM cylindrical panels rested on nonlinear elastic foundation. Taczała *et al.* (2022) investigated the nonlinear bending behavior, buckling and post-buckling response of generalized third-order FG plate. Belarbi *et al.* (2022) exploited extended layerwise theory to study the bending and free vibration of porous FG sandwich plate with various porosity distributions. Zhao *et al.* (2022) studied vibration characteristics of FG carbon nanotube-reinforced composite double-beams in thermal environments. Singh *et al.* (2022) developed an analytical solution for sound radiation of vibrating thin mode localized FG plates relative to physical neutral surface. Peng *et al.* (2022) studied the bending and free vibration of the stiffened FGM plate resting on Pasternak foundation by using the

moving Kriging approximation. Benguediab *et al.* (2023) examined the thermomechanical behavior of Macro and Nano FGM sandwich plates. Melaibari *et al.* (2022), Assie *et al.* (2023b) developed mathematical formulation to portray the bending response of BDFG porous plate resting on an elastic foundation. Esen *et al.* (2022) Abdelrahman *et al.* (2023) examined dynamic response of FG porous nanobeams subjected thermal and magnetic fields under moving load. Belounar *et al.* (2023) developed a novel four-node quadrilateral finite element to study the buckling and vibration of FGM plates. Alessi *et al.* (2023) studied the dynamic response of Piezoelectric Perforated Cantilever Bimorph Energy Harvester via Finite Element Analysis.

Many plate and shell structures in real applications are exposed to extensive thermal load and large displacements. Therefore, geometric nonlinearity statics analysis for investigation of the plate is always essential and cannot be neglected, Afzali *et al.* (2023). Kitipornchai *et al.* (2004) developed a semi-analytical solution for nonlinear vibration of laminated FGM plates with geometric imperfections. In 2007, Shen examined the nonlinear thermal bending response of shear deformable FG piezoelectric actuators plate under combined thermal and electrical loads. Li *et al.* (2007) studied the nonlinear thermomechanical post-buckling of FGM circular plate under mechanical non-uniform thermal loads. Nonlinear bending behavior of FG carbon nanotube reinforced composite plates are evaluated by three-dimensional element-free Galerkin method (Zhou and Song 2019) and generalized differential quadrature method (Keleshteri *et al.* 2019). She *et al.* (2020) examined forced resonance vibration of porous functionally graded (FG) curved nanobeam. Cho *et al.* (2022) used the natural element method to investigate Nonlinear bending analysis of FG-CNTRC plate resting on elastic foundation. Mahmoud *et al.* (2022) examined the thermo-mechanical bending response of porous FG sandwich plates via a simple integral plate model. Hoang and Thanh (2023) used Galerkin's method to predict the effect of Kerr foundation on nonlinear transient response of FG plate in thermal environment. Ding *et al.* (2023) presented a nonlinear low-velocity impact response of a graphene platelets-reinforced cylindrical shell with spinning motion. Siam *et al.* (2023) exploited Navier analytical method to study the free vibration analysis of nonlocal viscoelastic nanobeam with holes and elastic foundations. Baakeel *et al.* (2023) used a finite element ANSYS to examine the static and modal response of bio-inspired laminated composite shells. Mohamed *et al.* (2023a) used Bernstein polynomials method to investigate the nonlinear snap-through instability of helicoidal composite imperfect beams. Mohamed *et al.* (2023b) developed the novel incremental–iterative method capable of solving a nonlinear static response of BDFG porous plates. Hu *et al.* (2023) derived the analytical solutions for a free vibration of non-Lévy-type porous FGM plates within the symplectic framework.

Extended to previous work developed by Mohamed *et al.* (2023b), the following article aims to develop a nonlinear bending response of BDFG porous plate relative to neutral surface plane instead of mid-plane formulation. The rest of this manuscript is adopted as following: -Section 2 presents the kinematic and constitutive equations of BDFG porous plate, in addition to the equivalent stiffnesses relative to miplane and neural surface plane, respectively. The nonlinear equilibrium equations are derived in detail through section 2 and solved by differential/integral quadrature method (DIQM) in Section 3. Problem validation and convergence of incremental-iterative DQ method are presented in Section 4. Numerical results, parametric studies and discussions are developed through Section 5. Section 6 summarizes the main features of the following analysis and main points of the study.

2. Problem formulation

2.1 Geometrical and constitutive relations

As shown in Fig. 1, the displacement field of plate based on a neutral physical surface and a four variables high shear deformation theory without shear correction factors is described as (Zhang 2013, Shahverdi and Barati 2017, Babaei and Eslami 2021)

$$u(x,y,z) = u_o(x,y) - (z-z_o)\frac{\partial w_b}{\partial x} - (F(z)-c_o)\frac{\partial w_s}{\partial x} \tag{1a}$$

$$v(x,y,z) = v_o(x,y) - (z-z_o)\frac{\partial w_b}{\partial y} - (F(z)-c_o)\frac{\partial w_s}{\partial y} \tag{1b}$$

$$w(x,y,z) = w_b(x,y) + w_s(x,y) \tag{1c}$$

In which,

• u_o , v_o , w_b and w_s are the displacements defined at the considered surface.

• W_b and w_s stand for bending and shear parts, respectively.

• z_o and c_o are parameters that define neutral surface and are to be evaluated by (Assie *et al.* 2023b, Melaibari *et al.* 2022)

$$\begin{aligned} z_o &= \mu\frac{\int_{-h/2}^{h/2} zE(x,z,\phi_o)dz}{\int_{-h/2}^{h/2} E(x,z,\phi_o)dz}, \\ c_o &= \mu\frac{\int_{-h/2}^{h/2} F(z)E(x,z,\phi_o)dz}{\int_{-h/2}^{h/2} E(x,z,\phi_o)dz} \end{aligned} \tag{2}$$

where $E(x,z,\phi_o)$ is the distributed Young' modulus that will be identified by Eq. (7).

• μ is defined as a factor equals one for neutral plane and zero for geometrical mid-plane.

• $F(z)$ is a shape function that estimates the distribution of transverse shear stress/strain (τ_{xz}, τ_{yz}) and may take several forms. In this work: $F(\boldsymbol{z}) = \frac{\boldsymbol{4z^3}}{\boldsymbol{3h^2}}$, (Reddy 2007)

The strain-displacement relationships are presented as, (Mohamed *et al.* 2023b)

$$\varepsilon_x = \varepsilon_x^o - z\frac{\partial^2 w_b}{\partial x^2} - F(z)\frac{\partial^2 w_s}{\partial x^2} \tag{3a}$$

$$\varepsilon_y = \varepsilon_y^o - z\frac{\partial^2 w_b}{\partial y^2} - F(z)\frac{\partial^2 w_s}{\partial y^2} \tag{3b}$$

$$\gamma_{xy} = \gamma_{xy}^0 - z\left(2\frac{\partial^2 w_b}{\partial x\partial y}\right) - F(z)\left(2\frac{\partial^2 w_s}{\partial x\partial y}\right) \tag{3c}$$

$$\gamma_{yz} = G(z)\frac{\partial w_s}{\partial y} \tag{3d}$$

$$\gamma_{xz} = G(z)\frac{\partial w_s}{\partial x} \tag{3e}$$

where

$$\varepsilon_x^o = \frac{\partial u_0}{\partial x} + \frac{1}{2}\left(\frac{\partial \bar{w}}{\partial x}\right)^2 + z_{o,x}\frac{\partial w_b}{\partial x} + c_{o,x}\frac{\partial w_s}{\partial x} \tag{4a}$$

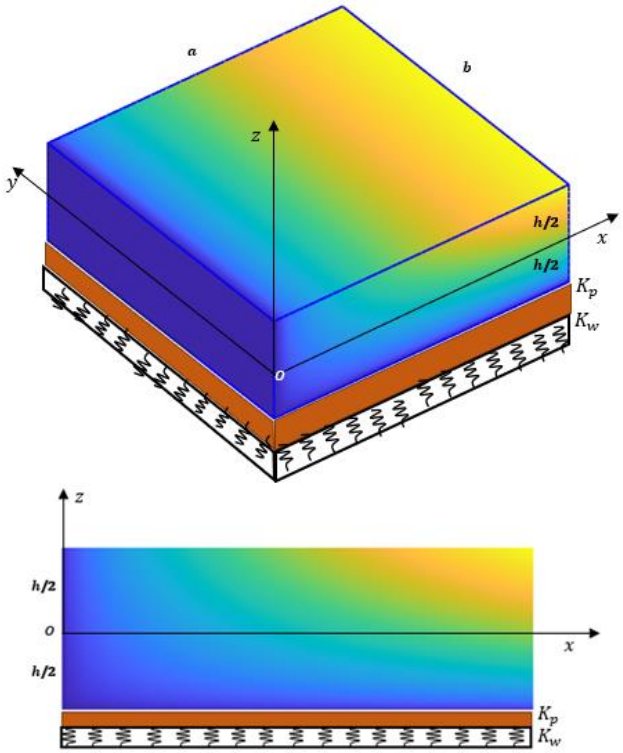

Fig. 1 Geometrical layout of 2D FG plate resting on elastic Winkler -Pasternak foundation with indices $n_x = n_z = 0.5$

$$\varepsilon_y^o = \frac{\partial v_0}{\partial y} + \frac{1}{2}\left(\frac{\partial \bar{w}}{\partial y}\right)^2 \tag{4b}$$

$$\gamma_{xy}^o = \frac{\partial u_o}{\partial y} + \frac{\partial v_o}{\partial x} + \frac{\partial \bar{w}}{\partial x}\frac{\partial \bar{w}}{\partial y} + z_{o,x}\frac{\partial w_b}{\partial y} + c_{o,x}\frac{\partial w_s}{\partial y} \tag{4c}$$

$$G(z) = 1 - F'(z) \tag{4d}$$

Based on equivalent single layer theory, which reduces the 3D problem to 2D shear deformation theory ($\varepsilon_z = 0$), the stress–strain relations can be characterized by (Mohamed *et al.* 2022)

$$\begin{bmatrix}\sigma_x\\ \sigma_y\\ \tau_{xy}\\ \tau_{yz}\\ \tau_{xz}\end{bmatrix} = \begin{bmatrix}Q_{11} & Q_{12} & 0 & 0 & 0\\ Q_{12} & Q_{22} & 0 & 0 & 0\\ 0 & 0 & Q_{66} & 0 & 0\\ 0 & 0 & 0 & Q_{44} & 0\\ 0 & 0 & 0 & 0 & Q_{55}\end{bmatrix}\begin{bmatrix}\varepsilon_x\\ \varepsilon_y\\ \gamma_{xy}\\ \gamma_{yz}\\ \gamma_{xz}\end{bmatrix} \tag{5}$$

In which the plane stress stiffnesses are (Mohamed *et al.* 2022)

$$\begin{gathered} Q_{11} = Q_{22} = \frac{E}{1-\nu^2}, \quad Q_{12} = \frac{\nu E}{1-\nu^2} \\ Q_{44} = Q_{55} = Q_{66} = \frac{E}{2(1+\nu)} \end{gathered} \tag{6}$$

According to power law function, the distribution of material properties, E with porosity through the thickness and axial directions are described by

$$E(x,z,\phi_o) = (E_m + (E_c - E_m)\left(\frac{1}{2}+\frac{z}{h}\right)^{n_z}\left(\frac{x}{a}\right)^{n_x}) \\ *[1-\Phi(z)] \tag{7}$$

where E is Young's modulus function that is varied through z -and x -directions by power function with indices, n_z and n_x, (Li *et al.* 2020). Subscripts c and m denote the ceramic and metal phases. h is the plate thickness and a is the plate length in x-direction. Poisson's ratio, ν is assumed to be constant for each constituent. $\Phi(z)$ is a porosity distribution that has the following three types (Coskun *et al.* 2019)

Type 1 (center enhanced):

$$\Phi(z) = \phi_o \cos\left(\frac{\pi}{\mathrm{h}}z\right) \tag{8a}$$

Type 2 (top enhanced):

$$\Phi(z) = \phi_o \cos\left(\frac{\pi}{2}\left(\frac{z}{h}+\frac{1}{2}\right)\right) \tag{8b}$$

Type 3 (bottom enhanced):

$$\Phi(z) = \phi_o \cos\left(\frac{\pi}{2}\left(\frac{z}{h}-\frac{1}{2}\right)\right) \tag{8c}$$

where: $\phi_o(=\varphi=\phi)$ is the porosity coefficient.

Equivalent stiffnesses based on midplane (MS), To consider the geometric middle surface of the plate, put z_o and c_o as zero − valued $(\mu = 0)$ in displacement and strain fields of Eqs. (1)-(4). Rigidities terms are obtained as functions of x as (Melaibari *et al.* 2022)

$$\left[A_{\mathrm{ij}}(x), B_{\mathrm{ij}}(x), D_{\mathrm{ij}}(x),\ B^s_{\mathrm{ij}}(x),\ D^s_{\mathrm{ij}}(x),\ H^s_{\mathrm{ij}}(x)\right] = \\ \int_{-h/2}^{h/2} Q_{\mathrm{ij}}(x,z,\phi_o)\ \left[1, z, z^2, F(z), zF(z), \left(F(z)\right)^2\right] dz \\ ij = 11,12,22,66 \tag{9a}$$

$$A^s_{\mathrm{ij}}(x) = \int_{-h/2}^{h/2} Q_{\mathrm{ij}}(x,z,\phi_o)(G(z))^2 dz \quad ij = 44,55 \tag{9b}$$

$Q_{ij}(x,z,\phi_o)$ and $E(x,z,\phi_o)$ are defined by Eqs. (6) and (7), respectively.

Equivalent stiffnesses based on neutral physical plane (NS): due to the use of z_o and c_o $(\mu = 1)$ defined by Eq. (3) in displacement field of Eq. (1), the plate stiffnesses $B_{ij}(x)$ and $B^s_{ij}(x)$ are zero-valued. Therefore, rigidity terms are modified as functions of x to (Assie *et al.* 2023b)

$$\left[A_{\mathrm{ij}}(x), D_{\mathrm{ij}}(x), D^s_{\mathrm{ij}}(x), H^s_{\mathrm{ij}}(x)\right] \\ = \int_{-h/2}^{h/2} Q_{\mathrm{ij}}(x,z,\phi_o)[1,(z-z_o)^2,(z-z_o)(F(z)-c_o),(F(z)-c_o)^2]\,dz \\ ij = 11,12,22,66 \tag{10a}$$

$$A^s_{\mathrm{ij}}(x) = \int_{-h/2}^{h/2} Q_{\mathrm{ij}}(x,z,\phi_o)(G(z))^2 dz \quad ij = 44,55 \tag{10b}$$

2.2 Hamilton's principles and governing equations

The governing equations of equilibrium and associated boundary conditions of the developed model are derived by using Hamilton's Principles (static version), which be described as

$$\int_0^T \delta\big(U + V + U_{ef}\big)dt = 0 \tag{11}$$

where the virtual potential work of applied loads can be expressed in the form, δV

$$\delta V = -\int_A q\delta\,(w_b + w_s)dA \tag{12}$$

and the variation of potential energy of the elastic foundation (Winkler -Pasternak type) can be expressed as

$$\delta U_{ef} = \int_A (K_w(w_b + w_s) - K_p\boldsymbol{\nabla^2}(w_b + w_s))\delta(w_b + w_s)dA$$

where:

$$\boldsymbol{\nabla^2}(w_b + w_s) = \frac{\partial^2(w_b+w_s)}{\partial x^2} + \frac{\partial^2(w_b+w_s)}{\partial y^2} \tag{13}$$

The virtual strain energy δU can be evaluated by

$$\delta U = \int_V \big(\sigma_x\delta\varepsilon_x + \sigma_y\delta\varepsilon_y + \tau_{xy}\delta\gamma_{xy} + \tau_{xz}\delta\gamma_{xz} + \tau_{yz}\delta\gamma_{yz}\big)dV \tag{14a}$$

in terms of stress resultants

$$\begin{aligned}\delta U = \int_A \Big[& N_x\delta\varepsilon_x^o + N_y\delta\varepsilon_y^o + N_{xy}\delta\gamma_{xy}^0 - M_x^b\frac{\partial^2\delta w_b}{\partial x^2} - M_y^b\frac{\partial^2\delta w_b}{\partial y^2} - M_{xy}^b\left(2\frac{\partial^2\delta w_b}{\partial x\partial y}\right) - \\ & M_x^s\frac{\partial^2\delta w_s}{\partial x^2} - M_y^s\frac{\partial^2\delta w_s}{\partial y^2} - M_{xy}^s\left(2\frac{\partial^2\delta w_s}{\partial x\partial y}\right) + S_{yz}^s\frac{\partial\delta w_s}{\partial y} + S_{xz}^s\frac{\partial\delta w_s}{\partial x}\Big]\ dA\end{aligned} \tag{14b}$$

Substituting Eqs. (12)-(14) for $\delta V, \delta U_{ef}$ and δU, respectively, into Eq. (11) and performing integration by parts, the following equilibrium equations are obtained

$$\delta u_o: \quad \frac{\partial N_x}{\partial x} + \frac{\partial N_{xy}}{\partial y} = 0 \tag{15a}$$

$$\delta v_o: \quad \frac{\partial N_{xy}}{\partial x} + \frac{\partial N_y}{\partial y} = 0 \tag{15b}$$

$$\delta w_b: \ \frac{\partial^2 M_x^b}{\partial x^2} + 2\frac{\partial^2 M_{xy}^b}{\partial x\partial y} + \frac{\partial^2 M_y^b}{\partial y^2} + \bar{N}_b(\bar{w}) + q + K_P\nabla^2(w_b + w_s) - K_w(w_b + w_s) = 0 \tag{15c}$$

$$\begin{aligned}\delta w_s: \ & \frac{\partial^2 M_x^s}{\partial x^2} + 2\frac{\partial^2 M_{xy}^s}{\partial x\partial y} + \frac{\partial^2 M_y^s}{\partial y^2} + \frac{\partial S_{yz}^s}{\partial y} + \frac{\partial S_{xz}^s}{\partial x} + \bar{N}_s(\bar{w}) + q + K_P\nabla^2(w_b + w_s) - \\ & K_w(w_b + w_s) = 0\end{aligned} \tag{15d}$$

and the boundary conditions

$$\delta u_o: \quad \big(N_x\bar{n}_x + N_{xy}\bar{n}_y\big)\delta u_0 = 0 \tag{16a}$$

$$\delta v_o: \quad \big(N_{xy}\bar{n}_x + N_y\bar{n}_y\big)\,\delta v_o = 0 \tag{16b}$$

$$\delta w_b: \ \Big(\big(M_{x,x}^b + M_{xy,y}^b\big)\bar{n}_x + \big(M_{xy,X}^b + M_{y,y}^b\big)\bar{n}_y + \bar{P}_b(\bar{w})\Big)\delta w_b = 0 \tag{16c}$$

$$\delta w_s: \quad \left(\left(M^s_{x,x}+M^s_{xy,y}+S^s_{xz}\right)\bar{n}_x+\left(M^s_{xy,X}+M^s_{y,y}+S^s_{yz}\right)\bar{n}_y+\bar{P}_s(\overline{w})\right)\delta w_s=0 \tag{16d}$$

$$\frac{\partial \delta w_b}{\partial x}: \quad \left(M^b_x\bar{n}_x+M^b_{xy}\bar{n}_y\right)\frac{\partial \delta w_b}{\partial x}=0 \tag{16e}$$

$$\frac{\partial \delta w_b}{\partial y}: \quad \left(M^b_{xy}\bar{n}_x+M^b_y\bar{n}_y\right)\frac{\partial \delta w_b}{\partial y}=0 \tag{16f}$$

$$\frac{\partial \delta w_s}{\partial x}: \quad \left(M^s_x\bar{n}_x+M^s_{xy}\bar{n}_y\right)\frac{\partial \delta w_s}{\partial x}=0 \tag{16g}$$

$$\frac{\partial \delta w_s}{\partial y}: \quad \left(M^s_{xy}\bar{n}_x+M^s_y\bar{n}_y\right)\frac{\partial \delta w_s}{\partial y}=0 \tag{16h}$$

The stress resultants can be expressed in a matrix form as

$$\begin{bmatrix} N_x \\ N_y \\ N_{xy} \\ M^b_x \\ M^b_y \\ M^b_{xy} \\ M^s_x \\ M^s_y \\ M^s_{xy} \end{bmatrix} = \begin{bmatrix} A_{11} & A_{12} & 0 & B_{11} & B_{12} & 0 & B^s_{11} & B^s_{12} & 0 \\ A_{12} & A_{22} & 0 & B_{12} & B_{22} & 0 & B^s_{12} & B^s_{22} & 0 \\ 0 & 0 & A_{66} & 0 & 0 & B_{66} & 0 & 0 & B^s_{66} \\ B_{11} & B_{12} & 0 & D_{11} & D_{12} & 0 & D^s_{11} & D^s_{12} & 0 \\ B_{12} & B_{22} & 0 & D_{12} & D_{22} & 0 & D^s_{12} & D^s_{22} & 0 \\ 0 & 0 & B_{66} & 0 & 0 & D_{66} & 0 & 0 & D^s_{66} \\ B^s_{11} & B^s_{12} & 0 & D^s_{11} & D^s_{12} & 0 & H^s_{11} & H^s_{12} & 0 \\ B^s_{12} & B^s_{22} & 0 & D^s_{12} & D^s_{22} & 0 & H^s_{12} & H^s_{22} & 0 \\ 0 & 0 & B^s_{66} & 0 & 0 & D^s_{66} & 0 & 0 & H^s_{66} \end{bmatrix} \begin{bmatrix} \varepsilon^o_x \\ \varepsilon^o_y \\ \gamma^0_{xy} \\ -\frac{\partial^2 w_b}{\partial^2 x} \\ -\frac{\partial^2 w_b}{\partial^2 y} \\ -\frac{2\partial^2 w_b}{\partial x \partial y} \\ -\frac{\partial^2 w_s}{\partial^2 x} \\ -\frac{\partial^2 w_s}{\partial^2 y} \\ -\frac{2\partial^2 w_s}{\partial x \partial y} \end{bmatrix} \tag{17a}$$

$$\begin{bmatrix} S^s_{yz} \\ S^s_{xz} \end{bmatrix} = \begin{bmatrix} A^s_{44} & 0 \\ 0 & A^s_{55} \end{bmatrix} \begin{bmatrix} \frac{\partial w_s}{\partial y} \\ \frac{\partial w_s}{\partial x} \end{bmatrix} \tag{17b}$$

By substituting Eqs. (3), (4) and (17) into Eq. (15), the above governing equations can be acquired in terms of generalized displacement (u_o, v_o, w_b, w_s) as (Mohamed *et al.* 2023)

$$\bar{N}_b(\overline{w}) = N(\overline{w}) + \left(\frac{\partial N_x}{\partial x}+\frac{\partial N_{xy}}{\partial y}\right)z_{o,x} + N_x z_{o,xx} \tag{18a}$$

$$\bar{N}_s(\overline{w}) = N(\overline{w}) + \left(\frac{\partial N_x}{\partial x}+\frac{\partial N_{xy}}{\partial y}\right)c_{o,x} + N_x c_{o,xx} \tag{18b}$$

$$\bar{P}_b(\overline{w}) = P(\overline{w}) + \left(N_x\bar{n}_x + N_{xy}\bar{n}_y\right)z_{o,x} \tag{18c}$$

$$\bar{P}_s(\overline{w}) = P(\overline{w}) + \left(N_x\bar{n}_x + N_{xy}\bar{n}_y\right)c_{o,x} \tag{18d}$$

$$N(\overline{w}) = \frac{\partial}{\partial x}\left(N_x\frac{\partial \overline{w}}{\partial x}+N_{xy}\frac{\partial \overline{w}}{\partial y}\right)+\frac{\partial}{\partial y}\left(N_{xy}\frac{\partial \overline{w}}{\partial x}+N_y\frac{\partial \overline{w}}{\partial y}\right) \tag{18e}$$

$$P(\overline{w}) = \left(N_x\frac{\partial \overline{w}}{\partial x}+N_{xy}\frac{\partial \overline{w}}{\partial y}\right)\bar{n}_x+\left(N_{xy}\frac{\partial \overline{w}}{\partial x}+N_y\frac{\partial \overline{w}}{\partial y}\right)\bar{n}_y \tag{18f}$$

Note that:

• The terms, $\bar{N}_b(\bar{w}), \bar{N}_s(\bar{w}), \bar{P}_b(\bar{w})$ and $\bar{P}_s(\bar{w})$, belong to large deformations.
• $\bar{w} = w_b + w_s$
• $\bar{w} = 0$ for linear analysis.
• The subscripts $_{,x}$ and $_{,xx}$ denote first- and second- derivative with respect to x.

3. Solution methodology

The governing equations consist of a set of four nonlinear partial differential equations. The assumption that the material properties change in the x-direction complicates the governing equations since they have variable-coefficients and consequently no analytical solution is available. In this work, the Differential/Integral Quadrature Method (DIQM) (Mohamed 2020, Mohamed *et al.* 2021, 2022) is developed to numerically solve the governing equations on a rectangular plate $(0 \le x \le a, 0 \le y \le b)$ with the following boundary conditions:

• Clamped edge as in Shanab *et al.* (2022)
• Two types of simply supported boundary conditions are considered: movable (SS1) and immovable (SS3) as in Melaibari *et al.* (2022)
• Modified simply supported boundary conditions are considered as in Melaibari *et al.* (2023).

3.1 DQM for partial differential equation

It was found that DIQM, developed by Mohamed *et al.* (2021) to solve linear/nonlinear integro-differential equations, provides highly accurate results with only few grid points. In this subsection, the details of DIQM for partial differential equations are presented.

Consider a partial differential equation in the unknown function $u(x, y)$. The 2D domain of the independent variables $0 < x < a,\ 0 < y < b$ is discretized by n and m points, respectively. The unknowns $u_{ij} = u(x_j, y_i), i = 1, \cdots, m, j = 1, \cdots, n$ defined on the rectangular domain are rearranged vector after vector to form the whole unknown vector.

$$\boldsymbol{U} = [u_{11}, u_{21}, \cdots u_{m1}, u_{12}, u_{22}, \cdots u_{m2}, \cdots, \cdots, u_{1n}, u_{2n}, \cdots u_{mn}]^T \tag{19}$$

Using classical definitions for DQM in one dimension (Shu (2012)), let D_x be the first order derivative matrix with respect to x of dimension $n \times n$ and let D_y be the first order derivative matrix with respect to y of dimension $m \times m$. To be consistent with the arrangement of unknowns given in Eq. (19) for vector U, the Kronecker product is used to construct global derivative matrices of dimension $(mn \times mn)$ as

$$\mathbb{D}_x = Kronecker(D_x, I(m)) \tag{20a}$$

$$\mathbb{D}_y = Kronecker(I(n), D_y) \tag{20b}$$

Where $I(n)$ and $I(m)$ are the identity matrices of dimensions $(n \times n)$ and $(m \times m)$, respectively. Based on Eq. (20), DQM can approximate higher and mixed partial derivatives such as $\frac{\partial^2 u}{\partial x^2}$, $\frac{\partial^2 u}{\partial y^2}$, $\frac{\partial^2 u}{\partial x \partial y}$ by $\mathbb{D}_{xx}U, \mathbb{D}_{yy}\,U$ and $\mathbb{D}_{xy}U$, respectively, where $\mathbb{D}_{xx} = \mathbb{D}_x^2$, $\mathbb{D}_{yy} = \mathbb{D}_y^2$, and $\mathbb{D}_{xy} = \mathbb{D}_x \mathbb{D}_y$. The governing equations for the BDFG plate consist of four variable-coefficient partial differential equations in the unknowns $u_0(x, y), v_0(x, y), w_b(x, y)$ and $w_s(x, y)$. They are discretized by DQM

as the unknown vectors U, V, W_b and W_s each of dimension $(nm \times 1)$. Moreover, the variable coefficients$A_{ij}(x), B_{ij}(x), D_{ij}(x), B^s_{ij}(x), D^s_{ij}(x), H^s_{ij}(x), ij = 11,12,22,66$ and $A^s_{ij}(x),\ ij = 44,55$, defined in Eqs. (9) and (10), can be computed by the integral quadrature method IQM, defined in (Mohamed *et al.* 2021), and arranged as $(nm \times 1)$ vectors $\mathcal{A}_{ij}, \mathcal{B}_{ij}, \mathcal{D}_{ij}, \mathcal{B}^s_{ij}, \mathcal{D}^s_{ij}, \mathcal{H}^s_{ij},\ i,j = 1,2,6$ and $\mathcal{A}^s_{44}, \mathcal{A}^s_{55}$, respectively (Mohamed *et al.* 2022). For convenience of applying DQM to discretize the variable-coefficient partial differential equations, a special matrices multiplication operator is introduced. The operator $'\circ'$ is defined such that for a vector $\mathcal{V}$ of dimensions $(n \times 1)$and a matrix $\mathcal{M}$ of dimensions $(n \times m)$ (i.e., each of $\mathcal{V}$ and $\mathcal{M}$ must have the same number of rows), $\mathcal{V} \circ \mathcal{M} = \mathcal{Y}$, implies that $\mathcal{Y}$ is a $(n \times m)$-matrix such that $\mathcal{Y}_{ij} = \mathcal{V}_i \mathcal{M}_{ij}$.

3.2 Linearization of the governing differential equations

The key assumption in the present linearization approach is that the nonlinear terms in the stress resultants, Eq. (17), and the nonlinear function $N(\bar{w})$ defined by Eq. (18) Neglecting derivatives of z_0 and c_0 with respect to x, are linearized by

$$\left(\frac{\partial \bar{w}}{\partial x}\right)^2 = \bar{w}_x \frac{\partial \bar{w}}{\partial x}\ ,\ \left(\frac{\partial \bar{w}}{\partial y}\right)^2 = \bar{w}_y \frac{\partial \bar{w}}{\partial y}\ ,\ \frac{\partial \bar{w}}{\partial x}\frac{\partial \bar{w}}{\partial y} = \bar{w}_x \frac{\partial \bar{w}}{\partial y} \tag{21}$$

In the proposed incremental-iterative method, the values of $\bar{w}_x = \frac{\partial \bar{w}^0}{\partial x}$ and $\bar{w}_y = \frac{\partial \bar{w}^0}{\partial y}$ are computed at some load-increment in the iteration step i such that $\bar{w}^0$ is defined by either of the following iteration methods (IM)

Classical IM:

$$\bar{w}^0 = \begin{cases} \bar{w}^* & \text{if } i = 1 \\ \bar{w}^{(i-1)} & \text{if } i > 1 \end{cases} \tag{22a}$$

Modified IM:

$$\bar{w}^0 = \begin{cases} \bar{w}^* & \text{if } i = 1 \\ \bar{w}^{(i-1)} & \text{if } i = 2 \\ (\bar{w}^{(i-2)} + \bar{w}^{(i-1)})/2 & \text{if } i > 2 \end{cases} \tag{22b}$$

where $\bar{w}^*$ is the transverse deflection at the previous load increment and $\bar{w}^{(i)}$ is the deflection at iteration i. Substituting Eq. (21) into Eq. (18) and applying the DQM, the stress resultants can be written as in

$$\begin{bmatrix} N_x \\ N_y \\ N_{xy} \\ M^b_x \\ M^b_y \\ M^b_{xy} \\ M^s_x \\ M^s_y \\ M^s_{xy} \end{bmatrix} = \begin{bmatrix} \mathcal{K}_{N_x} \\ \mathcal{K}_{N_y} \\ \mathcal{K}_{N_{xy}} \\ \mathcal{K}_{M^b_x} \\ \mathcal{K}_{M^b_y} \\ \mathcal{K}_{M^b_{xy}} \\ \mathcal{K}_{M^s_x} \\ \mathcal{K}_{M^s_y} \\ \mathcal{K}_{M^s_{xy}} \end{bmatrix} \mathcal{X} = [K_L + K_{NL}]\, \mathcal{X} \tag{23a}$$

where each of $\{\mathcal{K}_{N_x}, \mathcal{K}_{N_y}, \cdots, \mathcal{K}_{M^s_{xy}}\}$ is $(nm \times 4nm)$ matrix and

$$\mathcal{X} = \left[U^T, V^T, w_b^T, w_s^T\right]^T \tag{23b}$$

and K_L, K_{NL} are defined as in Mohamed et al (2023b).

Substitution of Eq. (23) in Eq. (15), the discretized linearized governing equations in a general iteration can be put in the form of

$$\begin{bmatrix} \mathbb{D}_x\, \mathcal{K}_{N_x} + \mathbb{D}_y\, \mathcal{K}_{N_{xy}} \\ \mathbb{D}_x\, \mathcal{K}_{N_{xy}} + \mathbb{D}_y\, \mathcal{K}_{N_y} \\ \mathbb{D}_{xx}\ \mathcal{K}_{M^b_x} + 2\mathbb{D}_{xy}\, \mathcal{K}_{M^b_{xy}} + \mathbb{D}_{yy}\ \mathcal{K}_{M^b_y} + \mathcal{N} + K_f \\ \mathbb{D}_{xx}\ \mathcal{K}_{M^s_x} + 2\mathbb{D}_{xy}\, \mathcal{K}_{M^s_{xy}} + \mathbb{D}_{yy}\ \mathcal{K}_{M^s_y} + \mathcal{N} + K_f + \mathbb{D}_y\, S^s_{yz} + \mathbb{D}_x\, S^s_{xz} \end{bmatrix} \boldsymbol{\mathcal{X}} = \boldsymbol{F} \tag{24a}$$

where F is the applied force vector of dimension $(4nm \times 1)$ and

$$\begin{gathered} \mathcal{N} = \mathbb{D}_x\left(\bar{\boldsymbol{w}}_{\boldsymbol{x}} \circ \mathcal{K}_{N_x} + \bar{\boldsymbol{w}}_{\boldsymbol{y}} \circ \mathcal{K}_{N_{xy}}\right) + \mathbb{D}_y\left(\bar{\boldsymbol{w}}_{\boldsymbol{x}} \circ \mathcal{K}_{N_{xy}} + \bar{\boldsymbol{w}}_{\boldsymbol{y}} \circ \mathcal{K}_{N_y}\right) \\ K_f = [O\ \ O\ \ f\ \ f]\,, \quad f = K_P\left(\mathbb{D}_{xx} + \mathbb{D}_{yy}\right) - K_w\, \mathbb{I}\,, \\ S^s_{yz} = \left[O\ \ O\ \ O\ \ \mathcal{A}^s_{44} \circ \mathbb{D}_y\right], \qquad S^s_{xz} = [O\ \ O\ \ O\ \ \mathcal{A}^s_{55} \circ \mathbb{D}_x] \end{gathered} \tag{24b}$$

In which O and $\mathbb{I}$ are the zero and identity matrices of dimensions $(mn \times \mathrm{m}n)$, respectively.

4. Validation and numerical results

In this section, accuracy and convergence of both of the proposed incremental-iterative solution methodology and the DIQM are analyzed and discussed as in Mohamed *et al.* (2023b). Several comparisons with existing literature which is limited only to through-thickness FGM plates are presented in the validation section 4.1. Influences of FG indexes, slenderness ratio, porosities and voids inside the material constituent and aspect ratio on deformation and stresses of BDFG plates are investigated in Section 4.2. The following non-dimensional parameters are defined as:

Non-dimensional maximum deflection: $\bar{w} = \frac{w_{max}}{h}$

Non-dimensional normal stress: $\bar{\sigma}_x = \sigma_x\left(\frac{a}{2}, \frac{b}{2}, \frac{h}{2}\right) \times \frac{a^2}{E_m\, h^2}$

Transverse load parameter: $\bar{q} = q_o \times \frac{a^4}{E_m\, h^4}$

The governing equations are presented for a rectangular plate $(0 \le x \le a, 0 \le y \le b)$ with the boundary conditions used in Shanab *et al.* (2022), Melaibari *et al.* (2022), Melaibari *et al.* (2023).

4.1 Model verification

4.1.1 Nonlinear isotropic plates

Table 1 presents the transverse central deflections of square isotropic plate under a uniform pressure calculated by present differential/integral quadrature method and compared with results of Talha and Singh (2011) using finite element method and Long *et al.* (2022) using Galerkin method, for SSSS, SCSC, and CCCC boundary conditions. As shown, very close results are obtained with slight deviations of less than 3%. In some times, the current results lay between the results of Long *et al.* (2022) and results of Talha and Singh (2011). Therefore, the precision and

Table 1 Non-dimensional central deflection $\bar{w}$ of square isotropic plate under different BCs and subjected to a uniform pressure

BCs	References	$\bar{q}$					
		4	8	12	16	20	40
SSSS	Talha and Singh (2011)	0.1200	0.2251	0.3185	0.3911	0.4597	0.6984
	Long *et al.* (2022)	0.1189	0.2254	0.3160	0.3927	0.4583	0.6908
	Present	0.1192	0.2260	0.3169	0.3939	0.4598	0.6938
SCSC	Talha and Singh (2011)	0.0602	0.1193	0.1764	0.2306	0.2811	0.4942
	Long *et al.* (2022)	0.0594	0.1179	0.1745	0.2286	0.2800	0.4953
	Present	0.0603	0.1199	0.1782	0.2349	0.2895	0.5286
CCCC	Talha and Singh (2011)	0.0405	0.0808	0.1207	0.1598	0.1981	0.3698
	Long *et al.* (2022)	0.0395	0.0788	0.1177	0.1560	0.1936	0.3681
	Present	0.0416	0.0830	0.1239	0.1640	0.2034	0.3834

Table 2 The non-dimensional central deflections and bending moment of immovable simply supported square isotropic porous plates under uniform load parameters

P		Type 1 porosity		Type 2 porosity		Type 3 porosity	
		Nonlinear	Linear	Nonlinear	Linear	Nonlinear	Linear
Central deflections $\bar{w}$							
5	Long *et al.* (2022) -DB	0.3025	0.3454	0.2593	0.2820	0.2970	0.3379
	Present	0.2915	0.3451	0.2568	0.2840	0.2869	0.3380
10	Long *et al.* (2022)-DB	0.4973	0.6908	0.4466	0.5640	0.4897	0.6758
	Present	0.4968	0.6902	0.4480	0.5680	0.4895	0.6760
15	Long *et al.* (2022)-DB	0.6325	1.0362	0.5826	0.8460	0.6238	1.0137
	Present	0.6318	1.0354	0.5836	0.8521	0.6233	1.0140
30	Long *et al.* (2022)-DB	0.8945	2.0724	0.8502	1.6920	0.8838	2.0275
	Present	0.8933	2.0707	0.8501	1.7041	0.8827	2.0280
Bending moment $M_x^b \times 10^6$							
5	Long *et al.* (2022)-DB	4.2317	4.8963	4.4656	4.8963	4.2484	4.8963
	Present	4.0772	4.9114	4.3986	4.9114	4.1002	4.9114
10	Long *et al.* (2022)-DB	6.8129	9.7926	7.5763	9.7926	6.8625	9.7926
	Present	6.8432	9.8228	7.5767	9.8228	6.8885	9.8228
15	Long *et al.* (2022)2-DB	8.5074	14.6888	9.7371	14.6888	8.5837	14.6888
	Present	8.5523	14.7342	9.7334	14.7342	8.6223	14.7342
30	Long *et al.* (2022)-DB	11.5594	29.3777	13.7264	29.3777	11.6863	29.3777
	Present	11.6455	29.4685	13.7312	29.4685	11.7632	29.4685

applicability of the proposed method have been proved through this example.

Table 2 illustrates the validation of the porosity models with previous work developed by Long *et al.* (2022). As shown, a comparison with for non-dimensional central deflections $\bar{w} = \left(\frac{w_{max}}{h}\right)$ and bending moment $\left(M_x^b \times 10^6\right)$ of immovable simply supported square isotropic porous plates under uniform load parameters $P = q_0 \times \left(\frac{a^4}{Eh^4}\right)$ based on neutral surface formulation (NS) with

Table 3 Comparison for non-dimensional central deflections of immovable simply supported square isotropic porous plates under uniform load parameters with and without elastic foundation

(K_w, K_s)		*P*=5	*P*=10	*P*=15	*P*=30
(0, 0)	Long *et al.* (2022)	0.2593	0.4466	0.5826	0.8502
	Present	0.2568	0.4480	0.5836	0.8501
(300, 0)	Long *et al.* (2022)	0.2483	0.4329	0.5687	0.8379
	Present	0.2467	0.4342	0.5696	0.8377
(300, 100)	Long *et al.* (2022)	0.2268	0.4047	0.5398	0.8119
	Present	0.2263	0.4058	0.5407	0.8118

different porosity models at the following properties:- $\left(E_c = E_m,\ \nu = \frac{1}{3}, \frac{a}{h} = 10, K_w = K_s = 0, \varphi = 0.5\right)$. From this table, it can be concluded that the deflections and bending moments obtained by linear case are generally overestimated than by nonlinear case. In addition, increasing applied load produces a wider gap between the two cases. As shown, the current results of deflections and bending moments are very close to those obtained by Long *et al.* (2022). The maximum deviation observed in case of bending moment at *P*=5 is around 3.7%.

To validate the elastic foundation model, Table 3 presents comparison with Long *et al.* (2022) for non-dimensional central deflections $\bar{w} = \left(\frac{w_{max}}{h}\right)$ of immovable simply supported square isotropic porous plates under uniform load parameters $P = q_0 \times \left(\frac{a^4}{Eh^4}\right)$ based on neutral surface formulation (NS). $\left(E_c = E_m = 200 \text{ MPa},\ \nu = \frac{1}{3}, \frac{a}{h} = 10, \varphi = 0.5 \text{ (Type 1)}\right)$ with and without elastic foundation $K_w = k_w \frac{a^4}{E_0 h^3}$ and $K_s = k_s \frac{a^2}{E_0 h^3 \nu}, E_0 = 1$ MPa). A decrease of deflection is noted in the increasing of elastic foundation because of increasing the plate stiffness. The influence of shear stiffness coefficients is more significant than transverse stiffness coefficients. As noticed, very close results are achieved with those published with Long *et al.* (2022).

4.1.2 Nonlinear bending analysis of 1D FG plate

This subsection is devoted to verifying the current 1D FGM model using linear analysis of NS formulation with previous published work. Using NS-formulation, the load- deflection curves of a simply supported SS3-FGM square plate (alumina/aluminum, *a/h*=100) under uniformly distributed load are compared for $n_x = 0, n_z = \{0, 0.5, 2, 10\}$ with Singha *et al.* (2011) in Fig. 2. The following properties are used $(n_x = 0, n_z = \{0, 0.5, 2, 10\}; \frac{a}{h} = 100)$ under immovable SS3 boundary conditions. $E_m = 70$ GPa, $E_c = 380$ GPa, $\nu = 0.3, \left(\hat{q} = q_0 \times \frac{12(1-\nu^2)a^4}{E_c h^4}\right)$. As shown, excellent agreement with previous work is obtained. As expected, the deflection increases when the value of n_z is increased since the plate stiffness decreases due to reduction of ceramic volume fraction ($n_z = 0$ corresponds to a full ceramic plate).

Fig. 3 presents a validation of non-dimensional deflection and axial stresses under uniform load of 1D FGM plate made of Ti-6Al-4V and aluminum oxide developed by NS model with Movable SSSS boundary conditions. As shown, the obtained results for central deflection and axial normal stresses $\hat{\sigma}_x$ are identical with those obtained by Van Do and Lee (2018). a comparison with Van

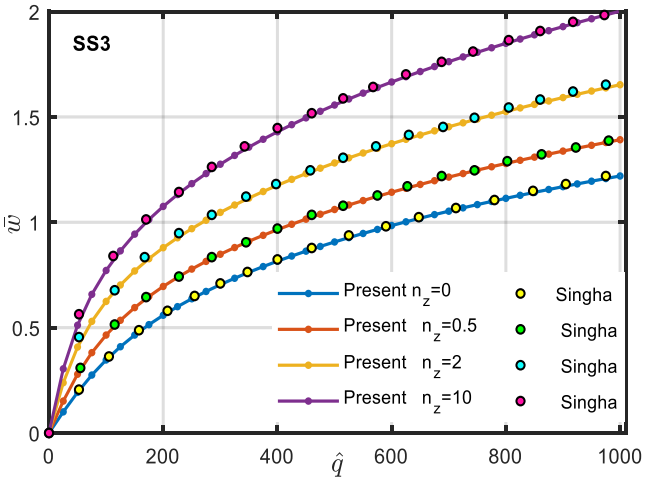

Fig. 2 Non-dimensional central displacement ($\overline{w} = \frac{w_{max}}{h}$) versus applied uniform transverse load of a FGM plate

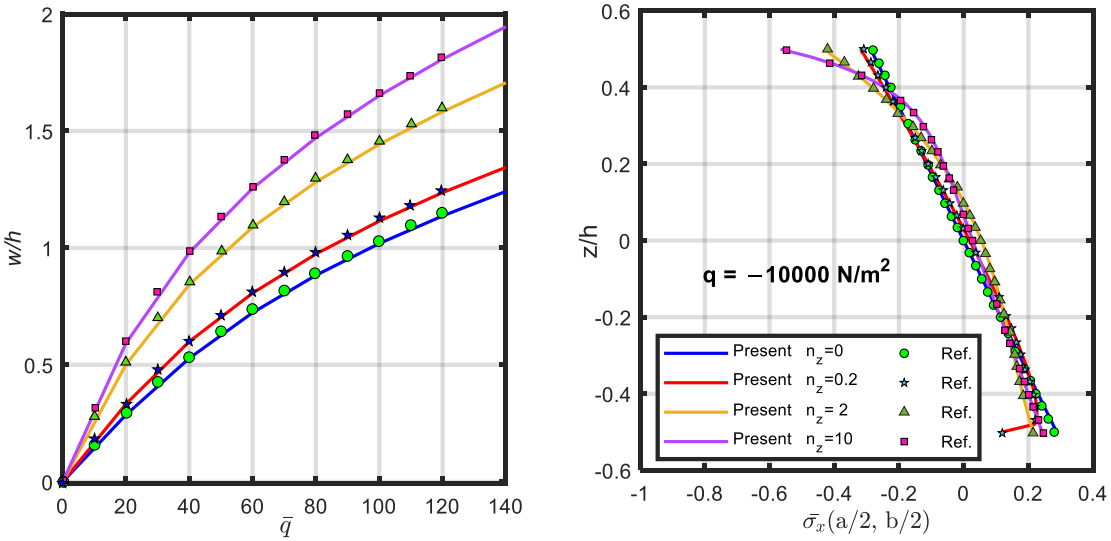

(a) Deflection-load curves (b) Axial stress through thickness

Fig. 3 Comparison with Van Do and Lee (2018) for (a) non-dimensional deflection versus transversal load and (b) axial stresses $\hat{\sigma}_x = \sigma_x\left(\frac{a}{2}, \frac{b}{2}, z\right)\frac{h^2}{|q_0|\, a^2}$ under uniform load $q_0 = -10000\,\frac{\mathrm{N}}{\mathrm{m}^2}$

Do and Lee (2018) for (a) non-dimensional deflection versus transversal load and (b) axial stresses $\hat{\sigma}_x = \sigma_x\left(\frac{a}{2}, \frac{b}{2}, z\right)\frac{h^2}{|q_0|\, a^2}$ under uniform load $q_0 = -10000\,\frac{\mathrm{N}}{\mathrm{m}^2}$.

4.2 Parametric analysis

Fig. 4 shows that compared with the MS-formulation, NS-formulation predicts higher values of

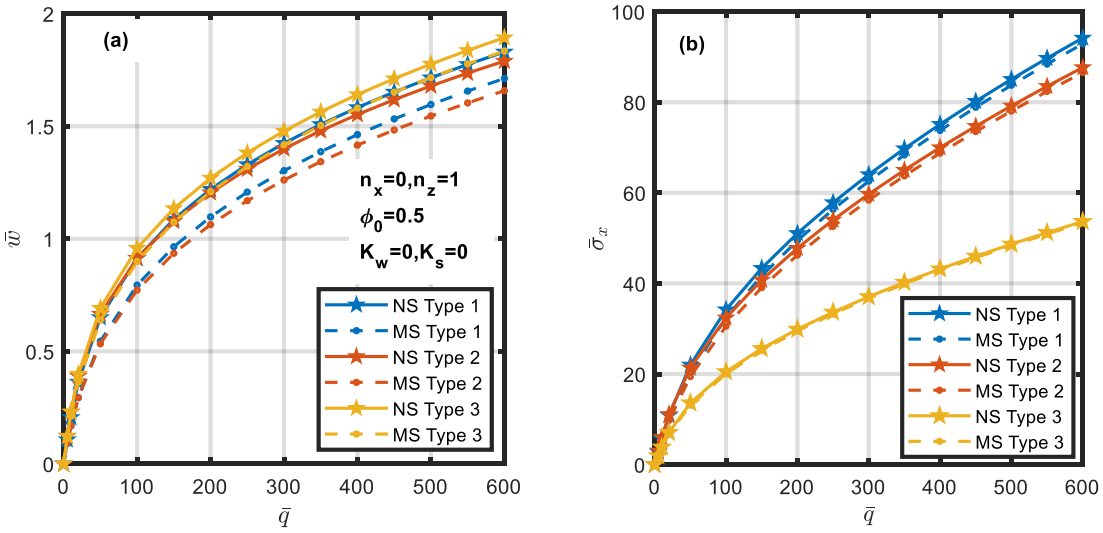

Fig. 4 Effect of porosity type ($\varphi_0 = 0.5$) on (a) dimensionless maximum deflection $\bar{w}$ and (b) axial stresses $\hat{\sigma}_x = \sigma_x\left(\frac{a}{2},\frac{b}{2},\frac{h}{2}\right)\frac{a^2}{E_m\,h^2}$ versus uniform transverse load $\bar{q}$ of a square FG plate ($n_z = 1, n_x = 0$) based on mid-surface MS and neutral-surface NS formulations assuming immovable SSSS-BCs. $\bar{w} = \frac{w}{h}, E_m = 70$ Gpa; $\nu_m = 0.3$; $E_c = 380$ GPa; $\nu_c = 0.3, \frac{a}{h} = 10, \bar{q} = q\frac{a^4}{E_m h^4}; n_z = 1, K_w = 0, K_s = 0$

$\bar{w}$ and $\hat{\sigma}_x$ for all considered porosity types. These response variations result due to the induced edge moments in case of MS formulation because of 1) the immovable SSSS-BCs ($N_x \neq 0$) and 2) the shift ($z_0 \neq 0, c_0 \neq 0$) between neutral- and mid-planes (since $n_z \neq 0$).

For more investigation on the combined influence of BDFG material and porosity distrbution, Table 4(a) and 4(b) present detailed results for $n_z = 0$ and $n_z = 1$, respectively while $n_x = \{0,1\}$ for different values of applied transverse load $\bar{q}$. The tabulated results consider various porosity types and parameters $\varphi_0 = \{0.2,0.5\}$. The case of $(n_z = 0, n_x = 0)$, the first set in Table 4(a), corresponds to a homogeneous porous plate and the following observations can easily be derived.

(a) Both of NS- and MS-formulations predict the same responses $(\bar{w}, \hat{\sigma}_x)$ for type-1 porosity since it is symmetric in the thickness direction and hence neutral- and mid- surfaces are coincident.

(b) The NS- formulation predicts identical values of $\bar{w}$ for both type-2 and type-3 porosity. However, the computed values of $\hat{\sigma}_x$ are different since $\hat{\sigma}_x$ is calculated at $z = \frac{h}{2}$ which is asymmetric with respect to the distribution of these porosity types.

(c) Due to the induced moments in the case of MS-formulation, it predicts different responses $(\bar{w}, \hat{\sigma}_x)$ for type-2 and type-3 porosity. That is because the induced moments, although being equal, they have opposite signs.

The second set of results in Table 4(a) presents responses of axially FG $(n_z = 0, n_x = 1)$porous plates. Since $n_z = 0$, the above three observations are still valid but the corresponding deflections $\bar{w}$ are increased because increasing n_x from $0 \rightarrow 1$ decreases the plate stiffness (in the x-direction).

The results reported in Table 4(b) present responses $(\bar{w}, \hat{\sigma}_x)$ of BDFG porous square plates.

Table 4(a) Effect of porosity (type and parameter) on dimensionless maximum deflection $\bar{w}$ and axial stresses $\hat{\sigma}_x = \sigma_x\left(\frac{a}{2},\frac{b}{2},\frac{h}{2}\right)\frac{a^2}{E_m h^2}$of a square BDFG plate under uniform transverse load $\bar{q}$ based on mid-surface MS and neutral-surface NS formulations with classical immovable SS-BCs. $\bar{w} = \frac{w}{h}, E_m = 70$ Gpa; $\nu_m = 0.3$; $E_c = 380$ GPa; $\nu_c = 0.3, \frac{a}{h} = 10, \bar{q} = q\frac{a^4}{E_m h^4}; n_z = 0, K_w = 0, K_s = 0$

n_x	Porosity Parameter ϕ_0	Formulation	Porosity Type	$\bar{w}$ $\bar{q}$=200	400	600	$\hat{\sigma}_x$ $\bar{q}$=200	400	600
0	0.2	NS	Perfect	0.8228	1.1164	1.3112	36.9045	54.2738	67.2308
			Type 1	0.8669	1.1722	1.3749	39.3568	57.9039	71.8132
			Type 2	0.8757	1.1788	1.3803	38.7866	56.9130	70.5624
			Type 3	0.8757	1.1788	1.3803	32.7436	47.7406	58.9735
		MS	Perfect	0.8228	1.1164	1.3112	36.9045	54.2738	67.2308
			Type 1	0.8669	1.1722	1.3749	39.3568	57.9039	71.8132
			Type 2	0.8565	1.1584	1.3598	38.4382	56.6099	70.3021
			Type 3	0.8955	1.1999	1.4017	33.0523	48.0074	59.2006
	0.5	NS	Type 1	0.9504	1.2784	1.4967	44.1044	65.0554	80.9162
			Type 2	0.9808	1.3008	1.5150	42.1377	61.6775	76.6663
			Type 3	0.9808	1.3008	1.5150	24.8466	35.6352	43.7850
		MS	Type 1	0.9504	1.2784	1.4967	44.1044	65.0554	80.9162
			Type 2	0.9200	1.2383	1.4528	41.1739	60.8835	75.9947
			Type 3	1.0483	1.3718	1.5865	25.5101	36.1625	44.2122
1	0.2	NS	Perfect	1.0710	1.4127	1.6428	28.0486	40.4793	49.9469
			Type 1	1.1252	1.4811	1.7211	29.9088	43.2349	53.4300
			Type 2	1.1325	1.4864	1.7254	29.4024	42.4641	52.4942
			Type 3	1.1325	1.4864	1.7254	24.7244	35.4965	43.7316
		MS	Perfect	1.0710	1.4127	1.6428	28.0486	40.4793	49.9469
			Type 1	1.1252	1.4811	1.7211	29.9088	43.2349	53.4300
			Type 2	1.1123	1.4659	1.7050	29.2259	42.3290	52.3850
			Type 3	1.1536	1.5080	1.7470	24.8793	35.6131	43.8236
	0.5	NS	Type 1	1.2283	1.6118	1.8710	33.5540	48.7123	60.3985
			Type 2	1.2535	1.6301	1.8860	31.8137	46.0800	57.2073
			Type 3	1.2535	1.6301	1.8860	18.5341	26.3420	32.3538
		MS	Type 1	1.2283	1.6118	1.8710	33.5540	48.7123	60.3985
			Type 2	1.1913	1.5683	1.8250	31.3473	45.7385	56.9349
			Type 3	1.3243	1.7022	1.9581	18.8413	26.5464	32.4957

Since $n_z \neq 0$, the neutral- and mid- surfaces are not coincident $(z_0 \neq 0, c_0 \neq 0)$ and the assumption of immovable BCs $(N_x \neq 0, N_y \neq 0)$ would induce edge moments in case of MS-formulation. This fact interprets the variation in reported responses produced by NS- and MS-formulations for all porosity types and even for the nonporous (perfect) plates. Results in Table 4(b) indicate that the induced edge moments in the MS- formulations decrease the plate responses compared with the NS- formulations. Generally, the plate responses increase with increasing load $\bar{q}$, material gradation indexes (n_z, n_x) and porosity parameter φ_0.

The response of a square BDFG plate under load intensity $\bar{q} = 400$ is computed based on the neutral surface NS formulation. Variation of the nonlinear static deflection $\bar{w}$ and normal stresses

Table 4(b) Effect of porosity (type and parameter) on dimensionless maximum deflection $\bar{w}$ and axial stresses $\hat{\sigma}_x = \sigma_x\left(\frac{a}{2},\frac{b}{2},\frac{h}{2}\right)\frac{a^2}{E_m\,h^2}$ of a square BDFG plate under uniform transverse load $\bar{q}$ based on mid-surface MS and neutral-surface NS formulations with classical immovable SS-BCs. $\bar{w} = \frac{w}{h}, E_m =$ 70 Gpa; $\nu_m = 0.3$; $E_c = 380$ GPa; $\nu_c = 0.3, \frac{a}{h} = 10, \bar{q} = q\frac{a^4}{E_m h^4}; n_z = 1, K_w = 0, K_s = 0$

n_x	Porosity Parameter ϕ_0	Formulation	Porosity Type	$\bar{w}$			$\hat{\sigma}_x$		
				$\bar{q}$=200	400	600	$\bar{q}$=200	400	600
0	0.2	NS	Perfect	1.0622	1.3868	1.6061	43.4155	63.2448	78.7331
			Type 1	1.1163	1.4540	1.6826	46.0353	67.2721	83.9389
			Type 2	1.1121	1.4450	1.6707	45.0376	65.7052	81.9637
			Type 3	1.1301	1.4700	1.7002	38.6925	56.2177	69.9529
		MS	Perfect	0.9566	1.2817	1.5027	42.0370	62.1550	77.7874
			Type 1	1.0051	1.3439	1.5745	44.5958	66.1095	82.9052
			Type 2	0.9931	1.3279	1.5561	43.5803	64.5570	80.9560
			Type 3	1.0368	1.3773	1.6090	37.7251	55.4537	69.2789
	0.5	NS	Type 1	1.2198	1.5831	1.8298	51.0481	75.1268	94.1789
			Type 2	1.2045	1.5520	1.7892	47.7787	69.9817	87.6668
			Type 3	1.2698	1.6407	1.8934	29.8823	43.1847	53.6686
		MS	Type 1	1.0972	1.4627	1.7121	49.4502	73.7604	92.8979
			Type 2	1.0631	1.4160	1.6576	46.2472	68.7572	86.5537
			Type 3	1.2090	1.5804	1.8338	29.4860	42.8543	53.3501
1	0.2	NS	Perfect	1.2513	1.6223	1.8752	32.6929	47.3652	58.9066
			Type 1	1.3127	1.6994	1.9634	34.7689	50.5382	62.9892
			Type 2	1.3110	1.6936	1.9552	33.9745	49.3456	61.5104
			Type 3	1.3255	1.7134	1.9786	29.0262	41.9843	52.2058
		MS	Perfect	1.1833	1.5551	1.8091	31.7340	46.4386	57.9805
			Type 1	1.2411	1.6289	1.8941	33.7453	49.5352	61.9760
			Type 2	1.2269	1.6112	1.8745	32.9643	48.3968	60.5719
			Type 3	1.2735	1.6622	1.9281	28.3025	41.2494	51.4471
	0.5	NS	Type 1	1.4301	1.8472	2.1327	38.8088	56.8042	71.1042
			Type 2	1.4235	1.8274	2.1043	36.1493	52.8047	66.0993
			Type 3	1.4758	1.8977	2.1888	22.2067	32.0055	39.8115
		MS	Type 1	1.3512	1.7700	2.0571	37.6337	55.6159	69.8784
			Type 2	1.3103	1.7186	2.0000	35.1216	51.8810	65.2507
			Type 3	1.4640	1.8862	2.1804	21.8145	31.5376	39.4001

$\hat{\sigma}_x = \sigma_x\left(\frac{a}{2},\frac{b}{2},\frac{h}{2}\right)\frac{a^2}{E_m\,h^2}$ for various elastic foundation constants (K_s, K_w) are presented in Table 5. It is observed that increasing either of the elastic foundation parameters adds more stiffness to the plate and hence reduces the deflection and normal stresses.

In the present parametric study, the NS-formulation is adopted to investigate the effect of the gradation indexes (n_x, n_z) on the linear and nonlinear bending deflection $\bar{w}$ versus load $\bar{q}$ considering different BCs ($\frac{a}{h} = 10, K_w = K_s = 0, \varphi_0 = 0$). The results are presented in Fig. 5 and Table 6 considering the following BCs: (a) movable SSSS, (b) immovable $\bar{S}\bar{S}\bar{S}\bar{S}$, (c) CCCC, and (d) CSCS. The results reveal that

Table 5 Influence of elastic foundation parameters (K_s, K_w) on $\bar{w}$ and $\bar{\sigma}_x$ for immovable simply supported SSSS- and CCCC- BDFG square plate based on neutral surface formulation NS. $(n_z = n_x = 1, \varphi_0 = 0, a/h = 10)$

BC	K_s	$\bar{w}$					$\hat{\sigma}_x$				
	↓	K_w →0	50	100	200	300	K_w →0	50	100	200	300
SSSS	0	1.6223	1.6137	1.6051	1.5880	1.5709	47.3652	46.9575	46.5514	45.7435	44.9417
	20	1.5622	1.5537	1.5452	1.5283	1.5114	44.7622	44.3685	43.9764	43.1972	42.4249
	40	1.5024	1.4941	1.4857	1.4690	1.4524	42.2350	41.8562	41.4791	40.7305	39.9893
	60	1.4432	1.4350	1.4267	1.4103	1.3940	39.7923	39.4292	39.0680	38.3516	37.6431
	80	1.3847	1.3767	1.3686	1.3526	1.3367	37.4422	37.0956	36.7511	36.0684	35.3941
	100	1.3273	1.3195	1.3116	1.2960	1.2806	35.1923	34.8629	34.5357	33.8879	33.2489
CCCC	0	1.4247	1.4169	1.4092	1.3938	1.3784	46.4918	46.1156	45.7411	44.9972	44.2602
	20	1.3605	1.3529	1.3453	1.3302	1.3152	43.5013	43.1407	42.7819	42.0699	41.3655
	40	1.2977	1.2903	1.2829	1.2683	1.2537	40.6390	40.2953	39.9536	39.2763	38.6071
	60	1.2367	1.2295	1.2224	1.2082	1.1941	37.9181	37.5925	37.2691	36.6286	35.9966
	80	1.1778	1.1709	1.1640	1.1503	1.1368	35.3492	35.0426	34.7383	34.1361	33.5427
	100	1.1212	1.1146	1.1080	1.0949	1.0820	32.9396	32.6525	32.3677	31.8048	31.2507

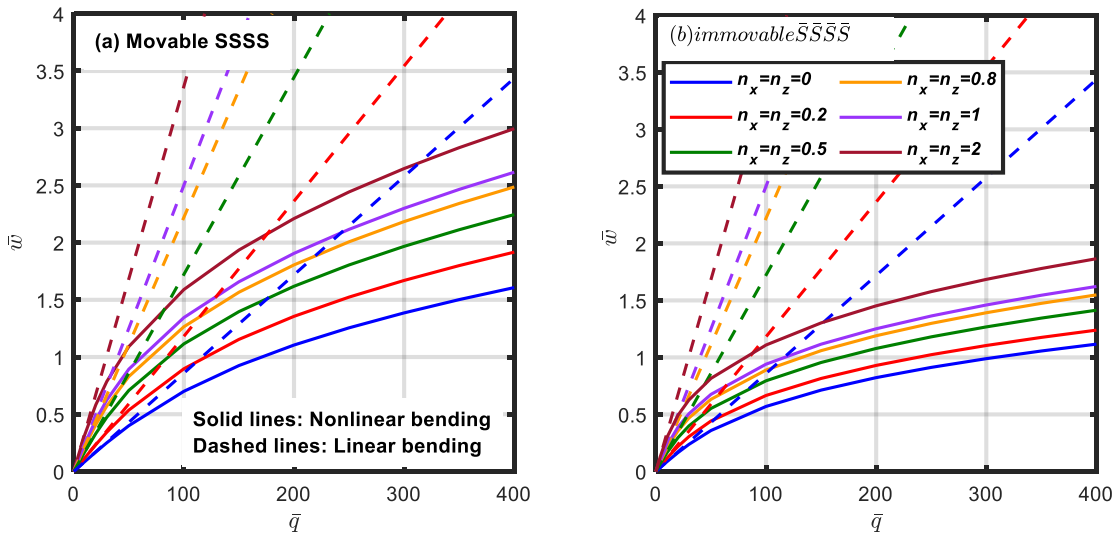

Fig. 5 Influence of material gradation indexes $n_x = n_z = \{0, 0.2, 0.5, 0.8, 1, 2\}$ on linear and nonlinear non-dimensional deflection $\bar{w}$ of a square BDFG plate (a/h=10) for different boundary conditions based on neutral surface formulation

• For all BCs, increasing the gradation indexes increases the dimensionless deflection due to the reduction of plate stiffness. This is true for both linear and nonlinear analyses.
• For all BCs, neglecting the nonlinear terms overestimates the deflection since these terms add more stiffness to the plate.
• The nonlinear bending deflections of the immovable simply supported BCs ($\bar{S}\bar{S}\bar{S}\bar{S}$) are considerably smaller than the movable-simply-supported BCs ($SSSS$) deflections. This is understood since the BCs of ($\bar{S}\bar{S}\bar{S}\bar{S}$) are more constrained than ($SSSS$) and hence they increase the plate stiffness.

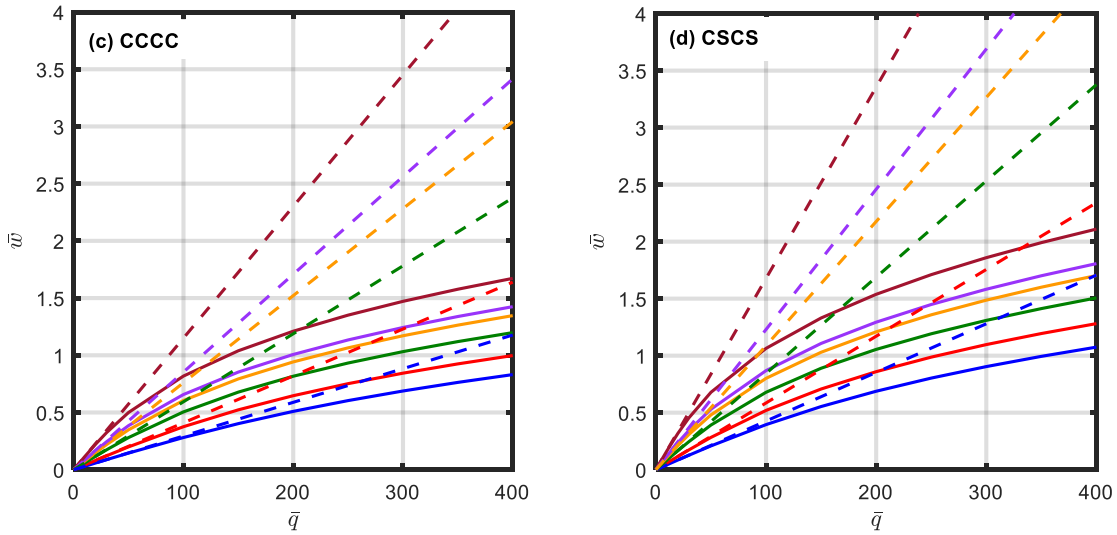

Fig. 5 Continued

Table 6 Influence of material gradation indexes (n_x, n_z) on linear $\bar{w}_L$ and nonlinear $\bar{w}_{NL}$ non-dimensional deflections of a square BDFG plate (a/h=10) for different boundary conditions based on neutral surface formulation

BCs	$(n_x = n_z)$ ↓	$\bar{q} = 100$		$\bar{q} = 300$		$\bar{q} = 500$	
		$\bar{w}_L$	$\bar{w}_{NL}$	$\bar{w}_L$	$\bar{w}_{NL}$	$\bar{w}_L$	$\bar{w}_{NL}$
Movable $SSSS$	0	0.8593	0.7004	2.5780	1.3858	4.2967	1.7927
	0.2	1.1815	0.8974	3.5446	1.6695	5.9077	2.1252
	0.5	1.7223	1.1150	5.1670	1.9672	8.6117	2.4802
	1	2.5013	1.3448	7.5040	2.3000	12.5066	2.8819
	2	3.3659	1.5898	10.0978	2.6471	16.8296	3.2900
	10	4.4742	1.8508	13.4226	3.0199	22.3710	3.7313
Immovable $\bar{S}\bar{S}\bar{S}\bar{S}$	0	0.8593	0.5700	2.5780	0.9891	4.2967	1.2212
	0.2	1.1815	0.6662	3.5446	1.1045	5.9077	1.3508
	0.5	1.7223	0.7950	5.1670	1.2676	8.6117	1.5357
	1	2.5013	0.9406	7.5040	1.4598	12.5066	1.7578
	2	3.3659	1.1087	10.0978	1.6844	16.8296	2.0172
	10	4.4742	1.2817	13.4226	1.9086	22.3710	2.2733
CCCC	0	0.2943	0.2811	0.8829	0.6877	1.4715	0.9508
	0.2	0.4098	0.3758	1.2293	0.8435	2.0489	1.1246
	0.5	0.5939	0.5052	1.7817	1.0319	2.9694	1.3349
	1	0.8539	0.6570	2.5616	1.2429	4.2693	1.5745
	2	1.1505	0.8185	3.4515	1.4713	5.7525	1.8381
	10	1.5226	0.9878	4.5679	1.6988	7.6131	2.0976
SCSC	0	0.4266	0.3953	1.2797	0.9042	2.1329	1.2164
	0.2	0.5853	0.5199	1.7558	1.0971	2.9263	1.4325
	0.5	0.8442	0.6790	2.5325	1.3094	4.2209	1.6729
	1	1.2298	0.8688	3.6893	1.5825	6.1488	1.9942
	2	1.6776	1.0640	5.0329	1.8594	8.3881	2.3189
	10	2.2535	1.2649	6.7604	2.1072	11.2673	2.5874

Contrarily, the linear bending deflections of the immovable ($\bar{S}\bar{S}\bar{S}\bar{S}$) and the movable ($SSSS$) BCs are identical. The reason is the bending-stretching uncoupling in the linear model based on the neutral-surface formulation. Since ($SSSS$) and ($\bar{S}\bar{S}\bar{S}\bar{S}$) are different only in the in-plane (stretching) BCs, the bending deflection is independent on these in-plane BCs.

5. Conclusions

In this article, the nonlinear static analysis of BDFG porous plate with mid-plane/neutral plane and moveable and immovable boundary conditions is presented. The higher order shear plate theory, mid-plane stretching with von Kármán large deformation, and elastic foundations are included in the model. The equilibrium nonlinear partial differential equations with variable coefficients are derived with associated boundary conditions for mid-pane and neutral plane. A novel incremental-iterative method with differential/integral quadrature method is exploited in the solution. The accuracy and applicability of the proposed method have been proved with many peers published works for nonlinear isotropic plate, elastic foundation, porosity and 1D FGM. Based on these analyses, it can concluded that: -

- The accuracy of proposed solution technique with incremental-iterative method and DIQM in solving nonlinear coupled partial differential equations with variable coefficients.
- The model can be applicable for thin, moderated thick, and thick plate including mid-plane or neutral surface formulation.
- The model can be used in analysis linear/nonlinear isotropic material, 1D FGM and 2D FGM including elastic foundations and porosity effects.
- For porosity type-1, both of NS- and MS-formulations predict the same responses ($\bar{w}, \hat{\sigma}_x$) since it is symmetric in the thickness direction and MS and NS are coincident.
- For both porosity type-2 and type-3, the NS- formulation predicts identical values of $\bar{w}$. However, the computed values of $\hat{\sigma}_x$ are different since $\hat{\sigma}_x$ is calculated at $z = h/2$ which is asymmetric with respect to the distribution of these porosity types.
- Increasing the elastic foundation parameters adds more stiffness to the plate and hence reduces the deflection and normal stresses.
- For all BCs, increasing the gradation indexes increases the dimensionless deflection due to the reduction of plate stiffness. This is true for both linear and nonlinear analyses.
- The nonlinear bending deflections of the immovable simply supported BCs ($\bar{S}\bar{S}\bar{S}\bar{S}$) are considerably smaller than the movable-simply-supported BCs ($SSSS$) deflections.

References

Abdelrahman, A.A., Esen, I., Daikh, A.A. and Eltaher, M.A. (2023), "Dynamic analysis of FG nanobeam reinforced by carbon nanotubes and resting on elastic foundation under moving load", *Mech. Bas. Des. Struct. Mach.*, **51**(10), 5383-5406. https://doi.org/10.1080/15397734.2021.1999263.

Afzali, M., Farrokh, M. and Carrera, E. (2023), "Nonlinear thermal post-buckling analysis of rectangular FG plates using CUF", *Compos. Struct.*, **321**, 117282. https://doi.org/10.1016/j.compstruct.2023.117282.

Alessi, Y.A., Ali, I.A., Alazwari, M.A., Almitani, K.H., Abdelrahman, A. and Eltaher, M.A. (2023), "Dynamic analysis of piezoelectric perforated cantilever bimorph energy harvester via finite element analysis", *Adv. Aircraft Spacecraft Sci.*, **10**(2), 179-202. https://doi.org/10.12989/aas.2023.10.2.179.

Alshorbagy, A.E., Eltaher, M.A. and Mahmoud, F. (2011), "Free vibration characteristics of a functionally

graded beam by finite element method", *Appl. Math. Model.*, **35**(1), 412-425. https://doi.org/10.1016/j.apm.2010.07.006.

Assie, A., Mohamed, S., Abdelrahman, A.A. and Eltaher, M.A. (2023b), "Mathematical formulations for static behavior of bi-directional FG porous plates rested on elastic foundation including middle/neutral-surfaces", *Steel Compos. Struct.*, **48**(2), 113-130. https://doi.org/10.12989/scs.2023.48.2.113.

Assie, A.E., Mohamed, S.M., Shanab, R.A., Abo-bakr, R.M. and Eltaher, M.A. (2023a), "Static buckling of 2D FG porous plates resting on elastic foundation based on unified shear theories", *J. Appl. Comput. Mech.*, **9**(1), 239-258. https://doi.org/10.22055/jacm.2022.41265.3723.

Attia, M.A., Melaibari, A., Shanab, R.A. and Eltaher, M.A. (2022), "Dynamic analysis of sigmoid bidirectional FG microbeams under moving load and thermal load: Analytical laplace solution", *Math.*, **10**(24), 4797. https://doi.org/10.3390/math10244797.

Baakeel, F., Eltaher, M.A., Basha, M.A., Melibati, A. and Abdelrahman, A.A. (2023), "Static and modal analysis of bio-inspired laminated composite shells using numerical simulation", *Adv. Aircraft Spacecraft Sci.*, **10**(4), 347-368. https://doi.org/10.12989/aas.2023.10.4.347.

Babaei, H. and Eslami, M.R. (2021), "Nonlinear analysis of thermal-mechanical coupling bending of FGP infinite length cylindrical panels based on PNS and NSGT", *Appl. Math. Model.*, **91**, 1061-1080. https://doi.org/10.1016/j.apm.2020.10.004.

Babaei, H., Kiani, Y. and Eslami, M.R. (2019), "Large amplitude free vibrations of long FGM cylindrical panels on nonlinear elastic foundation based on physical neutral surface", *Compos. Struct.*, **220**, 888-898. https://doi.org/10.1016/j.compstruct.2019.03.064.

Belarbi, M.O., Daikh, A.A., Garg, A., Hirane, H., Houari, M.S.A., Civalek, Ö. and Chalak, H.D. (2022), "Bending and free vibration analysis of porous functionally graded sandwich plate with various porosity distributions using an extended layerwise theory", *Arch. Civil Mech. Eng.*, **23**(1), 15. https://doi.org/10.1007/s43452-022-00551-0.

Belounar, A., Boussem, F. and Tati, A. (2023), "A novel C0 strain-based finite element for free vibration and buckling analyses of functionally graded plates", *J. Vib. Eng. Technol.*, **11**(1), 281-300. https://doi.org/10.1007/s42417-022-00577-x.

Benguediab, S., Kebir, T., Kettaf, F.Z., Daikh, A.A, Tounsi, A., Benguediab, M. and Eltaher, M.A. (2023), "Thermomechanical behavior of Macro and Nano FGM sandwich plates", *Adv. Aircraft Spacecraft Sci.*, **10**(1) 83-106. https://doi.org/10.12989/aas.2023.10.1.083.

Cho, J.R. (2022), "Nonlinear bending analysis of FG-CNTRC plate resting on elastic foundation by natural element method", *Eng. Anal. Bound. Elem.*, **141**, 65-74. https://doi.org/10.1016/j.enganabound.2022.05.008.

Coskun, S., Kim, J. and Toutanji, H. (2019), "Bending, free vibration, and buckling analysis of functionally graded porous micro-plates using a general third-order plate theory", *J. Compos. Sci.*, **3**(1), 15. https://doi.org/10.3390/jcs3010015.

Daikh, A.A., Belarbi, M.O., Khechai, A., Li, L., Khatir, S., Abdelrahman, A.A. and Eltaher, M.A. (2023), "Bending of Bi-directional inhomogeneous nanoplates using microstructure-dependent higher-order shear deformation theory", *Eng. Struct.*, **291**, 116230. https://doi.org/10.1016/j.engstruct.2023.116230.

Ding, H.X., Eltaher, M.A. and She, G.L. (2023), "Nonlinear low-velocity impact of graphene platelets reinforced metal foams cylindrical shell: Effect of spinning motion and initial geometric imperfections", *Aerosp. Sci. Technol.*, **140**, 108435. https://doi.org/10.1016/j.ast.2023.108435.

Eltaher, M.A., Abdelrahman, A.A., Al-Nabawy, A., Khater, M. and Mansour, A. (2014), "Vibration of nonlinear graduation of nano-Timoshenko beam considering the neutral axis position", *Appl. Math. Comput.*, **235**, 512-529. http://doi.org/10.1016/j.amc.2014.03.028.

Eltaher, M.A., Alshorbagy, A.E. and Mahmoud, F.F. (2013), "Determination of neutral axis position and its effect on natural frequencies of functionally graded macro/nanobeams", *Compos. Struct.*, **99**, 193-201. http://doi.org/10.1016/j.compstruct.2012.11.039.

Esen, I. (2019a), "Dynamic response of a functionally graded Timoshenko beam on two-parameter elastic foundations due to a variable velocity moving mass", *Int. J. Mech. Sci.*, **153**, 21-35. https://doi.org/10.1016/j.ijmecsci.2019.01.033.

Esen, I. (2019b), "Dynamic response of functional graded Timoshenko beams in a thermal environment subjected to an accelerating load", *Eur. J. Mech.-A/Solid.*, **78**, 103841. https://doi.org/10.1016/j.euromechsol.2019.103841.

Esen, I., Alazwari, M.A., Eltaher, M.A. and Abdelrahman, A.A. (2022), "Dynamic response of FG porous nanobeams subjected thermal and magnetic fields under moving load", *Steel Compos. Struct.*, **42**(6), 805-826. https://doi.org/10.12989/scs.2022.42.6.805.

Esen, I., Koc, M.A. and Cay, Y. (2018), "Finite element formulation and analysis of a functionally graded Timoshenko beam subjected to an accelerating mass including inertial effects of the mass", *Lat. Am. J. Solid. Struct.*, **15**, e119. https://doi.org/10.1590/1679-78255102.

Farzam, A. and Hassani, B. (2022), "Isogeometric analysis of FG polymer nanocomposite plates reinforced with reduced graphene oxide using MCST", *Adv. Aircraft Spacecraft Sci.*, **9**(1), 69-93. https://doi.org/10.12989/aas.2022.9.1.069.

Fernando, D., Wang, C.M. and Chowdhury, A.R. (2018), "Vibration of laminated-beams based on reference-plane formulation: Effect of end supports at different heights of the beam", *Eng. Struct.*, **159**, 245-251. https://doi.org/10.1016/j.engstruct.2018.01.004.

Gupta, S. and Chalak, H.D. (2022), "Prediction of vibration response of functionally graded sandwich plates by zig-zag theory", *Adv. Aircraft Spacecraft Sci.*, **9**(6), 507. https://doi.org/10.12989/aas.2022.9.6.507.

Haciyev, V.C., Sofiyev, A.H. and Kuruoglu, N. (2018), "Free bending vibration analysis of thin bidirectionally exponentially graded orthotropic rectangular plates resting on two-parameter elastic foundations", *Compos. Struct.*, **184**, 372-377. http://doi.org/10.1016/j.compstruct.2017.10.014.

Hoang, V.N.V. and Thanh, P.T. (2023), "Influences of arbitrary-distributed Kerr foundation on free vibration and nonlinear transient response of functionally graded plate in thermal environment", *Thin Wall. Struct.*, **188**, 110802. https://doi.org/10.1016/j.tws.2023.110802.

Hong, N.T. (2020), "Nonlinear static bending and free vibration analysis of bidirectional functionally graded material plates", *Int. J. Aerosp. Eng.*, **20**, 1-16. https://doi.org/10.1155/2020/8831366.

Hu, Z., Shi, Y., Xiong, S., Zheng, X. and Li, R. (2023), "New analytic free vibration solutions of non-Lévy-type porous FGM rectangular plates within the symplectic framework", *Thin Wall. Struct.*, **185**, 110609. https://doi.org/10.1016/j.tws.2023.110609.

Huynh, T.A., Lieu, X.Q. and Lee, J. (2017), "NURBS-based modeling of bidirectional functionally graded Timoshenko beams for free vibration problem", *Compos. Struct.*, **160**, 1178-1190. http://doi.org/10.1016/j.compstruct.2016.10.076.

Karamanli, A., Aydogdu, M. and Vo, T.P. (2021), "A comprehensive study on the size-dependent analysis of strain gradient multi-directional functionally graded microplates via finite element model", *Aerosp. Sci. Technol.*, **111**, 106550. https://doi.org/10.1016/j.ast.2021.106550.

Karamanli, A., Eltaher, M.A., Thai, S. and Vo, T.P. (2023), "Transient dynamics of 2D-FG porous microplates under moving loads using higher order finite element model", *Eng. Struct.*, **278**, 115566. https://doi.org/10.1016/j.engstruct.2022.115566.

Keleshteri, M.M., Asadi, H. and Aghdam, M.M. (2019), "Nonlinear bending analysis of FG-CNTRC annular plates with variable thickness on elastic foundation", *Thin Wall. Struct.*, **135**, 453-462. https://doi.org/10.1016/j.tws.2018.11.020.

Kitipornchai, S., Yang, J. and Liew, K.M. (2004), "Semi-analytical solution for nonlinear vibration of laminated FGM plates with geometric imperfections", *Int. J. Solid. Struct.*, **41**(9-10), 2235-2257. https://doi.org/10.1016/j.ijsolstr.2003.12.019.

Kumar, R., Singh, B.N., Singh, J. and Singh, J. (2022), "Meshfree approach for flexure analysis of bidirectional porous FG plate subjected to I, L, and T types of transverse loading", *Aerosp. Sci. Technol.*, **129**, 107824. https://doi.org/10.1016/j.ast.2022.107824.

Lezgy-Nazargah, M. (2015), "Fully coupled thermo-mechanical analysis of bi-directional FGM beams using NURBS isogeometric finite element approach", *Aerosp. Sci. Technol.*, **45**, 154-164. https://doi.org/10.1016/j.ast.2015.05.006.

Li, J., Wang, G., Guan, Y., Zhao, G., Lin, J., Naceur, H. and Coutellier, D. (2021), "Meshless analysis of bi-directional functionally graded beam structures based on physical neutral surface", *Compos. Struct.*, **259**,

113502. https://doi.org/10.1016/j.compstruct.2020.113502.
Li, S.R., Zhang, J.H. and Zhao, Y.G. (2007), "Nonlinear thermomechanical post-buckling of circular FGM plate with geometric imperfection", *Thin Wall. Struct.*, **45**(5), 528-536. https://doi.org/10.1016/j.tws.2007.04.002.
Long, N.V., Tu, T.M., Truong, H.Q., Hai, L.T. and Trang, V.T.T. (2022), "Displacement-based and stress-based analytical approaches for nonlinear bending analysis of functionally graded porous plates resting on elastic substrate", *Acta Mechanica*, **233**(4), 1689-1714. https://doi.org/10.1007/s00707-022-03196-5.
Mahmoud, S.R., Ghandourah, E., Algarni, A., Balubaid, M., Tounsi, A. and Bourada, F. (2022), "On thermo-mechanical bending response of porous functionally graded sandwich plates via a simple integral plate model", *Arch. Civil Mech, Eng.*, **22**(4), 186. https://doi.org/10.1007/s43452-022-00506-5.
Melaibari, A., Mohamed, S.A., Assie, A.E., Shanab, R.A. and Eltaher, M.A. (2022), "Static response of 2D FG porous plates resting on elastic foundation using midplane and neutral surfaces with movable constraints", *Math.*, **10**(24), 4784. https://doi.org/10.3390/math10244784.
Melaibari, A., Mohamed, S.A., Assie, A.E., Shanab, R.A. and Eltaher, M.A. (2023), "Free vibration characteristics of bidirectional graded porous plates with elastic foundations using 2D-DQM", *Math.*, **11**(1), 46. https://doi.org/10.3390/math11010046.
Mohamed, S., Assie, A.E., Mohamed, N. and Eltaher, M.A. (2022), "Static and stress analyses of bi-directional FG porous plate using unified higher order kinematics theories", *Steel Compos. Struct.*, **45**(3), 305-330. https://doi.org/10.12989/scs.2022.45.3.305.
Mohamed, S.A. (2020), "A fractional differential quadrature method for fractional differential equations and fractional eigenvalue problems", *Math. Meth. Appl. Sci*., https://doi.org/10.1002/mma.6753.
Mohamed, S.A., Assie, A.E. and Eltaher, M.A. (2023b), "Novel incremental procedure in solving nonlinear static response of 2D-FG porous plates", *Thin Wall. Struct.*, **189**, 110779. https://doi.org/10.1016/j.tws.2023.110779.
Mohamed, S.A., Mohamed, N., Abo-bakr, R.M. and Eltaher, M.A. (2023a), "Multi-objective optimization of snap-through instability of helicoidal composite imperfect beams using Bernstein polynomials method", *Appl. Math. Model.*, **120**, 301-329. https://doi.org/10.1016/j.apm.2023.03.034.
Mohamed, S.A., Mohamed, N.A. and Abo-Hashem, S.I. (2021), "A novel differential-integral quadrature method for the solution of nonlinear integro-differential equations", *Math. Meth. Appl. Sci.*, **44**(18), 13945-13967. https://doi.org/10.1002/mma.7667.
Nguyen, K., Thai, H.T. and Vo, T. (2015), "A refined higher-order shear deformation theory for bending, vibration and buckling analysis of functionally graded sandwich plates", *Steel Compos. Struct.*, **18**(1), 91-120. https://doi.org/10.12989/scs.2015.18.1.091.
Nguyen, N.V., Nguyen, H.X., Lee, S. and Nguyen-Xuan, H. (2018), "Geometrically nonlinear polygonal finite element analysis of functionally graded porous plates", *Adv. Eng. Softw.*, **126**, 110-126. https://doi.org/10.1016/j.advengsoft.2018.11.005.
Patil, M.A. and Kadoli, R. (2022), "Effect of porosity and gradation of Galfenol-D on vibration suppression of bidirectional functionally graded beam", *Mater. Today: Proc.*, **66**, 1870-1874. https://doi.org/10.1016/j.matpr.2022.05.412.
Peng, L.X., Chen, S.Y., Wei, D.Y., Chen, W. and Zhang, Y.S. (2022), "Static and free vibration analysis of stiffened FGM plate on elastic foundation based on physical neutral surface and MK method", *Compos. Struct.*, **290**, 115482. https://doi.org/10.1016/j.compstruct.2022.115482.
Qian, L.F. and Ching, H.K. (2004), "Static and dynamic analysis of 2-D functionally graded elasticity by using meshless local petrov-galerkin method", *J. Chin. Inst. Eng.*, **27**(4), 491-503. https://doi.org/10.1080/02533839.2004.9670899.
Ramteke, P.M. and Panda, S.K. (2023), "Nonlinear static and dynamic response prediction of bidirectional doubly-curved porous FG panel and experimental validation", *Compos. Part A: Appl. Sci. Manuf.*, **166**, 107388. https://doi.org/10.1016/j.compositesa.2022.107388.
Shahverdi, H. and Barati, M.R. (2017), "Vibration analysis of porous functionally graded nanoplates", *Int. J. Eng. Sci.*, **120**, 82-99. https://doi.org/10.1016/j.ijengsci.2017.06.008.
Shanab, R., Mohamed, S., Tharwan, M.Y., Assie, A.E. and Eltaher, M.A. (2022), "Buckling of 2D FG

Porous unified shear plates resting on elastic foundation based on neutral axis", *Steel Compos. Struct.*, **45**(5), 729. https://doi.org/10.12989/scs.2022.45.5.729.

Shanab, R.A. and Attia, M.A. (2022), "Semi-analytical solutions for static and dynamic responses of bi-directional functionally graded nonuniform nanobeams with surface energy effect", *Eng. Comput.*, **38**, 2269–2312. https://doi.org/10.1007/s00366-020-01205-6.

She, G.L., Liu, H.B. and Karami, B. (2020), "On resonance behavior of porous FG curved nanobeams", *Steel Compos. Struct.*, **36**(2), 179-186. https://doi.org/10.12989/scs.2020.36.2.179.

Shen, H.S. (2007), "Nonlinear thermal bending response of FGM plates due to heat conduction", *Compos. Part B: Eng.*, **38**(2), 201-215. https://doi.org/10.1016/j.compositesb.2006.06.004.

Shu, C. (2012), *Differential Quadrature and its Application in Engineering*, Springer Science & Business Media.

Siam, O.A., Shanab, R.A., Eltaher, M.A. and Mohamed, N.A. (2023), "Free vibration analysis of nonlocal viscoelastic nanobeam with holes and elastic foundations by Navier analytical method", *Adv. Aircraft Spacecraft Sci.*, **10**(3), 257-279. https://doi.org/10.12989/aas.2023.10.3.257.

Singh, B.N., Ranjan, V. and Hota, R.N. (2022), "Vibroacoustic response of mode localized thin functionally graded plates using physical neutral surface", *Compos. Struct.*, **287**, 115301. https://doi.org/10.1016/j.compstruct.2022.115301.

Singha, M.K., Prakash, T. and Ganapathi, M. (2011), "Finite element analysis of functionally graded plates under transverse load", *Finite Elem. Anal. Des.*, **47**(4), 453-460. https://doi.org/10.1016/j.finel.2010.12.001.

Taczała, M., Buczkowski, R. and Kleiber, M. (2022), "Analysis of FGM plates based on physical neutral surface using general third-order plate theory", *Compos. Struct.*, **301**, 116218. https://doi.org/10.1016/j.compstruct.2022.116218.

Talha, M. and Singh, B.N. (2011), "Nonlinear mechanical bending of functionally graded material plates under transverse loads with various boundary conditions", *Int. J. Model. Simul. Scientif. Comput.*, **2**(02), 237-258. https://doi.org/10.1142/S1793962311000451.

Van Do, T., Doan, D.H., Duc, N.D. and Bui, T.Q. (2017), "Phase-field thermal buckling analysis for cracked functionally graded composite plates considering neutral surface", *Compos. Struct.*, **182**, 542-548. http://doi.org/10.1016/j.compstruct.2017.09.059.

Van Do, V.N. and Lee, C.H. (2018), "Nonlinear analyses of FGM plates in bending by using a modified radial point interpolation mesh-free method", *Appl. Math. Model.*, **57**, 1-20. https://doi.org/10.1016/j.apm.2017.12.035.

Xu, J.Q., She, G.L., Li, Y.P. and Gan, L.L. (2023), "Nonlinear resonances of nonlocal strain gradient nanoplates made of Functionally graded materials considering geometric imperfection", *Steel Compos. Struct.*, **46**(6), 795-811. https://doi.org/10.12989/scs.2023.47.6.795.

Yin, S., Yu, T. and Liu, P. (2013), "Free vibration analyses of FGM thin plates by isogeometric analysis based on classical plate theory and physical neutral surface", *Adv. Mech. Eng.*, **5**, 634584. http://doi.org/10.1155/2013/634584.

Zhang, D.G. (2013), "Modeling and analysis of FGM rectangular plates based on physical neutral surface and high order shear deformation theory", *Int. J. Mech. Sci.*, **68**, 92-104. http://doi.org/10.1016/j.ijmecsci.2013.01.002.

Zhang, D.G. and Zhou, Y.H. (2008), "A theoretical analysis of FGM thin plates based on physical neutral surface", *Comput. Mater. Sci.*, **44**(2), 716-720. https://doi.org/10.1016/j.commatsci.2008.05.016.

Zhao, J.L., Chen, X., She, G.L., Jing, Y., Bai, R.Q., Yi, J., Pu, H.Y. and Luo, J. (2022), "Vibration characteristics of functionally graded carbon nanotube-reinforced composite double-beams in thermal environments", *Steel Compos. Struct.*, **43**(6), 797-808. https://doi.org/10.12989/scs.2022.43.6.797.

Zhou, T. and Song, Y. (2019), "Three-dimensional nonlinear bending analysis of FG-CNTs reinforced composite plates using the element-free Galerkin method based on the SR decomposition theorem", *Compos. Struct.*, **207**, 519-530. https://doi.org/10.1016/j.compstruct.2018.09.026.